THE ASTROPHYSICAL JOURNAL, 362:191–201, 1990 October 10

THE COMPACT MOLECULAR CORE TOWARD G34.3+0.2: VLA OBSERVATIONS IN THE (2, 2) AND (3, 3) LINES OF AMMONIA

GUIDO GARAY
Departamento de Astronomía, Universidad de Chile

AND

LUIS F. RODRÍGUEZ
Harvard-Smithsonian Center for Astrophysics; and Instituto de Astronomía, UNAM
Received 1989 April 3; accepted 1990 April 4

ABSTRACT

We present observations of the $(J, K) = (2, 2)$ and $(J, K) = (3, 3)$ inversion transitions of ammonia, made at 3″ resolution with the VLA, in the direction of the warm molecular cloud associated with the compact H II region G34.3+0.2. The main hyperfine (HF) line of the (2, 2) transition is detected in absorption toward the west and in emission toward the east of the warm cloud. The main HF line of the (3, 3) transition is detected in emission across the whole source. The satellite HF lines of the (2, 2) and (3, 3) lines are observed only in emission. Our data reveal the presence of three distinct regions, with the temperature and density of the gas increasing as the size of the region decreases.

The absorption feature arises in a low-density, $n(H_2) \sim 10^4$ cm^{-3}, low-temperature, $T_{rot} \sim 18$ K, gas in front of the brightest H II region within the complex. We suggest that this gas is part of the extended molecular material, mapped by Heaton and colleagues in 1985, that surrounds the compact H II regions. The (3, 3) main-line emission, which samples warm gas, arises in a molecular disklike structure $\sim 7\farcs3 \times 2\farcs8$ in size, elongated in a direction oriented $\sim 55°$ west of north. The emission in the satellite HF lines of the (2, 2) and (3, 3) transitions arises from an ultracompact region, of $\sim 1\farcs6$ in size, located at the center of the warm cloud and displaced $\sim 2''$ to the east of the head of the bright cometary H II region. The rotational temperature of the ammonia emission rises from ~ 70 K at the edge of the disklike structure to about 185 K at the central position. The molecular hydrogen density in the ultracompact core, of $\sim 7 \times 10^7$ cm^{-3}, is ~ 100 times higher than the density in the warm halo.

We suggest that the warm cloud corresponds to a disk of molecular gas that was formed from the collapse of a massive, rotating fragment embedded in an extended molecular cloud. Most of the mass at the center of this disk collapsed to form a massive star that ionizes the dense gas around it, producing a bright thermal radio source. The dense molecular gas near the recently formed star, heated and compressed by the associated compact H II region, gives rise to the molecular emission from the hot ultracompact core.

Subject headings: interstellar: molecules — nebulae: H II regions — nebulae: individual (G34.3+0.2) — radio sources: lines — stars: formation

I. INTRODUCTION

G34.3+0.2 is an H II region complex at a distance of 3.8 kpc projected $\sim 40'$ from the supernova remnant W44. Radio continuum observations made with angular resolution of $\sim 10''$ show four components spread over a region $\sim 60''$ in size (Turner *et al.* 1974; Garay, Reid, and Moran 1985). Interferometric radio continuum observations, with arcsecond angular resolution, show that the most compact of these components has a cometary shape, with a head approximately 4″ in size and a 20″ tail trailing to the west, and that, in addition to the four components, there are two weak and small H II regions (Reid and Ho 1985; Garay, Rodríguez, and van Gorkom 1986). These results indicate that a cluster of OB stars, which excite the H II regions, was recently formed toward G34.3+0.2. Several other signs of active star formation, such as H_2O and OH maser emission, are also present toward this region (Genzel and Downes 1977; Garay, Reid, and Moran 1985; Gaume and Mutel 1987).

Molecular line observations of the (1, 1) and (2, 2) inversion transition of ammonia toward G34.3+0.2, with a resolution of 40″, show the presence of a *molecular cloud core*, of $\sim 90''$ in diameter (1.7 pc at the distance of 3.8 kpc) having a molecular hydrogen density of 4×10^4 cm^{-3} and an excitation temperature of 18 K, which is embedded in a low-density, extended envelope (Heaton *et al.* 1985). Andersson and Garay (1986), observing the (3, 3) inversion transition of ammonia with the VLA, detected, near the center of the core, a dense and warm molecular clump, also referred to as the *compact core*, which is closely associated with the brightest compact H II region within the complex. The size of the compact core is ~ 0.1 pc, and the excitation temperature of the (3, 3) line is ~ 60 K. Dense molecular cores around ultracompact H II regions are thought to be remnants of the gas from which the OB stars formed, and therefore they are useful objects for studying the physical parameters and dynamics of the gas in the earliest stages of star formation.

In a multilevel study of the molecular gas associated with G34.3+0.2, with an angular resolution of $\sim 40''$, Henkel, Wilson, and Mauersberger (1987) detected emission from several highly excited NH_3 inversion transitions and concluded that it arises from molecular gas that has an NH_3 column density of 3×10^{18} cm^{-2} and a kinetic temperature of ~ 225 K. In addition, they conclude that the structure of this gas, which is most likely part of the compact core, should be

complex, exhibiting small scale clumping. Keto, Ho, and Reid (1987, hereafter KHR) observed with the VLA the NH_3 (1, 1) transition toward the compact core in G34.3+0.2. The spectrum shows a weak emission component and a strong absorption feature, which they suggest arises from molecular gas that is gravitationally collapsing onto the compact H II region.

We report here observations of the (2, 2) and (3, 3) inversion transitions of NH_3 made with angular resolution of $\sim 3''$. The purpose of these observations is twofold. First, they permit a determination of the spatial structure of the compact molecular core. Second, they permit a more accurate estimation of the physical parameters of the molecular gas associated with G34.3+0.2. After this paper was submitted for publication we became aware of a paper by Heaton, Little, and Bishop (1989) reporting VLA observations of the (3, 3) transition of ammonia from G34.3+0.2, made with an angular resolution of $\sim 1''$. Their results are in good agreement with ours.

II. OBSERVATIONS

The observations were made with the Very Large Array of the National Radio Astronomical Observatory.[1] The array was in the D configuration, which provides a shortest spacing of 40 m and a longest spacing of 1000 m. The phase center of the array was set at $\alpha(1950) = 18^h50^m46^s.17$ and $\delta(1950) = 1°11'12''.6$.

We observed the $(J, K) = (2, 2)$ and $(J, K) = (3, 3)$ inversion transitions of ammonia toward G34.3+0.2 on 1986 January 23. We assumed rest frequencies of 23722.633 and 23870.129 MHz for the (2, 2) and (3, 3) transitions, respectively. The synthesized beams were $3''.0 \times 2''.9$ P.A. $-52°$ and $3''.2 \times 3''.0$ P.A. $-53°$ at the frequencies of the (2, 2) and (3, 3) lines, respectively. We used a bandpass of 12.5 MHz, centered at an LSR velocity of 55 km s^{-1}, and 31 spectral channels 195.3 KHz wide each (about 2.5 km s^{-1} at the observing frequencies). The integration time on source was ~ 160 and 110 minutes for the (2, 2) and (3, 3) transitions, respectively, with 25 antennas. Each 12 minute scan on-source was paired with a 3 minute calibration scan on 1749+096. The data were edited and calibrated by applying the complex gain solution from the calibration source. The flux density scale was determined by observing 3C 286 for which we assumed a flux density of 2.4 Jy at 1.3 cm. The spectral data were further calibrated by applying the solution obtained from a self-calibration on the continuum channel, which contains the average of the central 75% of the bandpass, using the algorithm of Schwab (1980). The rms noise level in a single spectral line channel was 15 and 17 mJy per beam solid angle for the (2, 2) and (3, 3) observations, respectively. To convert to brightness temperature, the fluxes in mJy per beam should be multiplied by 0.244 and 0.226 for the (2, 2) and (3, 3) observations, respectively.

III. RESULTS

a) Continuum Map

Figure 1 shows the radio continuum map in the direction of G34.3+0.2 made using the continuum channel of the (2, 2) NH_3 line observations. The bright cometary-like H II region and the two weaker compact sources toward the east of it, as observed by Reid and Ho (1985) at 1.6 GHz with an angular resolution of 1".4 and by Garay, Rodríguez, and van Gorkom (1986) at 14.7 GHz with an angular resolution of 0".4, are clearly detected in this map. However, they appear blended due to the larger beam size of our observations. We also see some of the weak emission toward the SE reported by Reid and Ho (1985). The total integrated flux densities contained in the 23.7 and 23.9 GHz maps are the same, 5.3 ± 0.1 Jy. Therefore, errors in the ratio of intensities of the (2, 2) and (3, 3) lines due to uncertainties in the flux calibration are negligible. The uncertainty in the absolute flux density scale is difficult to estimate. Andersson and Garay (1986) measured a total flux density at 23.9 GHz of 5.4 ± 0.4 Jy, whereas Heaton *et al.* (1989) measured a flux of 5.2 Jy. The good agreement between measurements suggests that the flux densities are probably accurate to 5%.

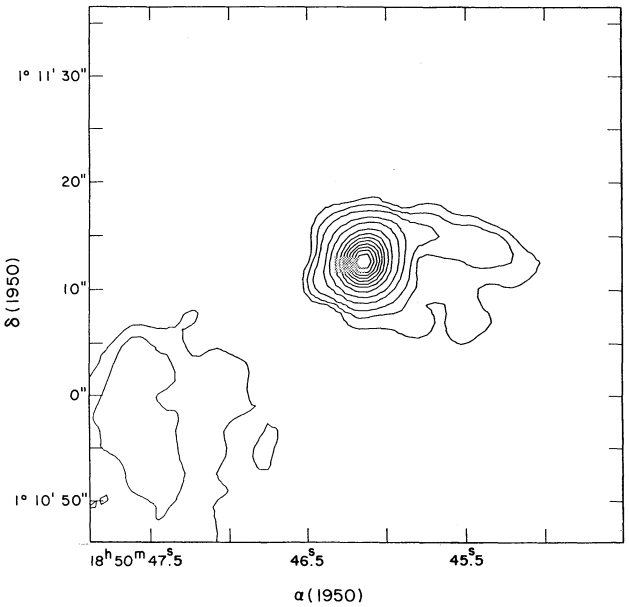

FIG. 1.—VLA continuum map of the compact H II region G34.3+0.2 at 23.7 GHz with 3" resolution. Contour levels are -0.5, 0.5, 1, 2, 5, 10, 20, 30, 40, 50, 60, 70, 80, and 90% of the peak brightness of 3.09 Jy $beam^{-1}$.

b) Line Profiles

The (2, 2) and (3, 3) inversion lines of NH_3 are split, due to the hyperfine interaction of the electric quadrupole moment of the N nucleus with the electric field of the electrons, into five components consisting of a central main line and two pairs of satellite lines symmetrically placed about the main line. In the absence of non–LTE effects and in the optically thin limit, the satellite lines should have an intensity of $\sim 5\%$ and $\sim 3\%$ of the main line for the (2, 2) and (3, 3) transitions, respectively.

Figure 2 shows the line profiles of the (2, 2) and (3, 3) inversion lines of NH_3 over an $11'' \times 10''$ region covering the ammonia emission. The pixel size is 0".8. The profiles of the (2, 2) and (3, 3) lines are strikingly different. The main and satellite HF lines of the (3, 3) transition are detected in emission throughout the whole source. The strong intensity of the satellite lines, at ± 21.5 km s^{-1} and ± 28.9 km s^{-1} from the main line, indicate that these lines have significant optical depth. In the case of the (2, 2) inversion transition, the main HF line is detected in emission toward the east and in absorption toward the west, while the satellite HF lines, at ± 16.6 km s^{-1} and ± 25.8 km s^{-1}, are detected only in emission.

[1] The National Radio Astronomy Observatory is operated by Associated Universities Inc., under cooperative agreement with the National Science Foundation.

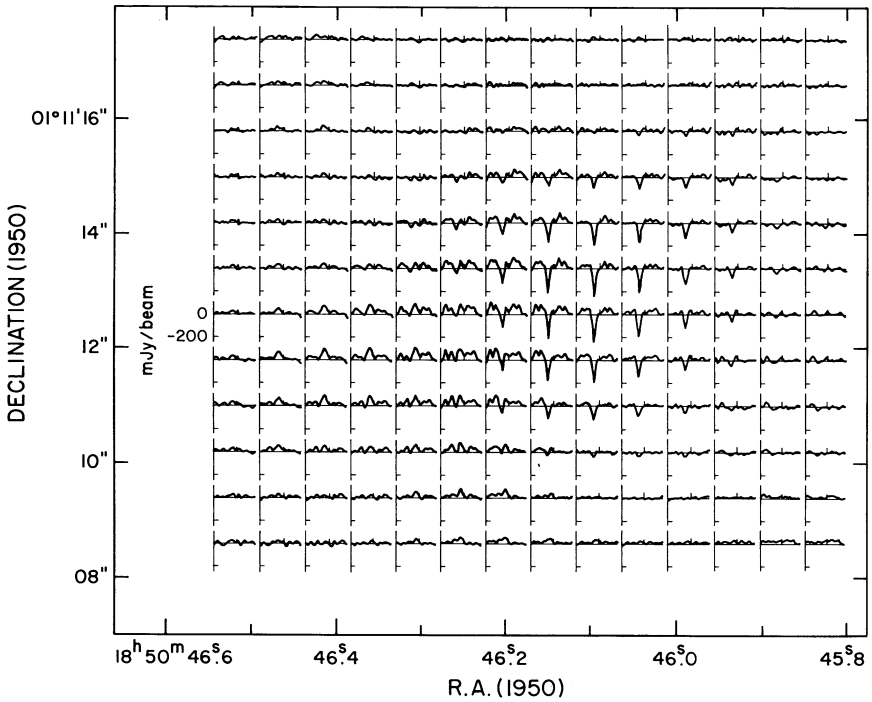

FIG. 2a

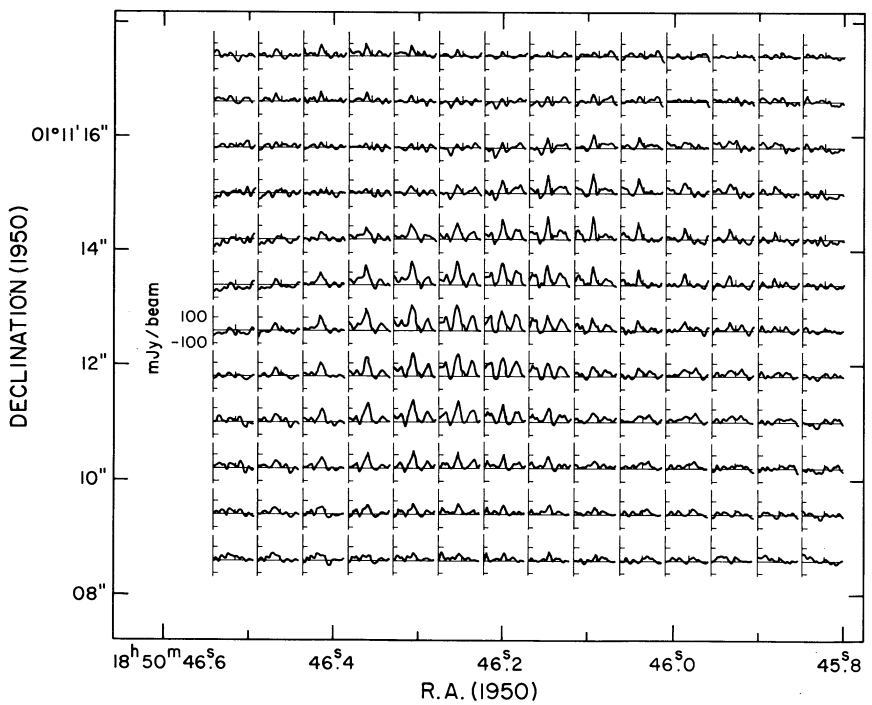

FIG. 2b

FIG. 2.—(*a*) Beam-averaged profiles of the (2, 2) line of ammonia. The velocity scale increases from 18.0 to 92.0 km s^{-1}, right to left. (*b*) Beam-averaged profiles of the (3, 3) line of ammonia. The velocity scale increases from 18.2 to 91.8 km s^{-1}, right to left.

c) Line Maps

The line maps presented below were made from the individual channel maps by subtracting a continuum map made from the average of off-line channel maps. Figure 3 shows the individual line maps of the (2, 2) inversion transition of NH_3 in the velocity range from 92.0 km s^{-1} to 18.0 km s^{-1}; the channel width is 2.47 km s^{-1}. The main results that can be extracted from these maps are the following. First, the central line maps (velocities 55.0 to 64.9), which cover the range of velocities expected for the main HF line, exhibit two distinct regions: an eastern region, which shows NH_3 in emission, and a western

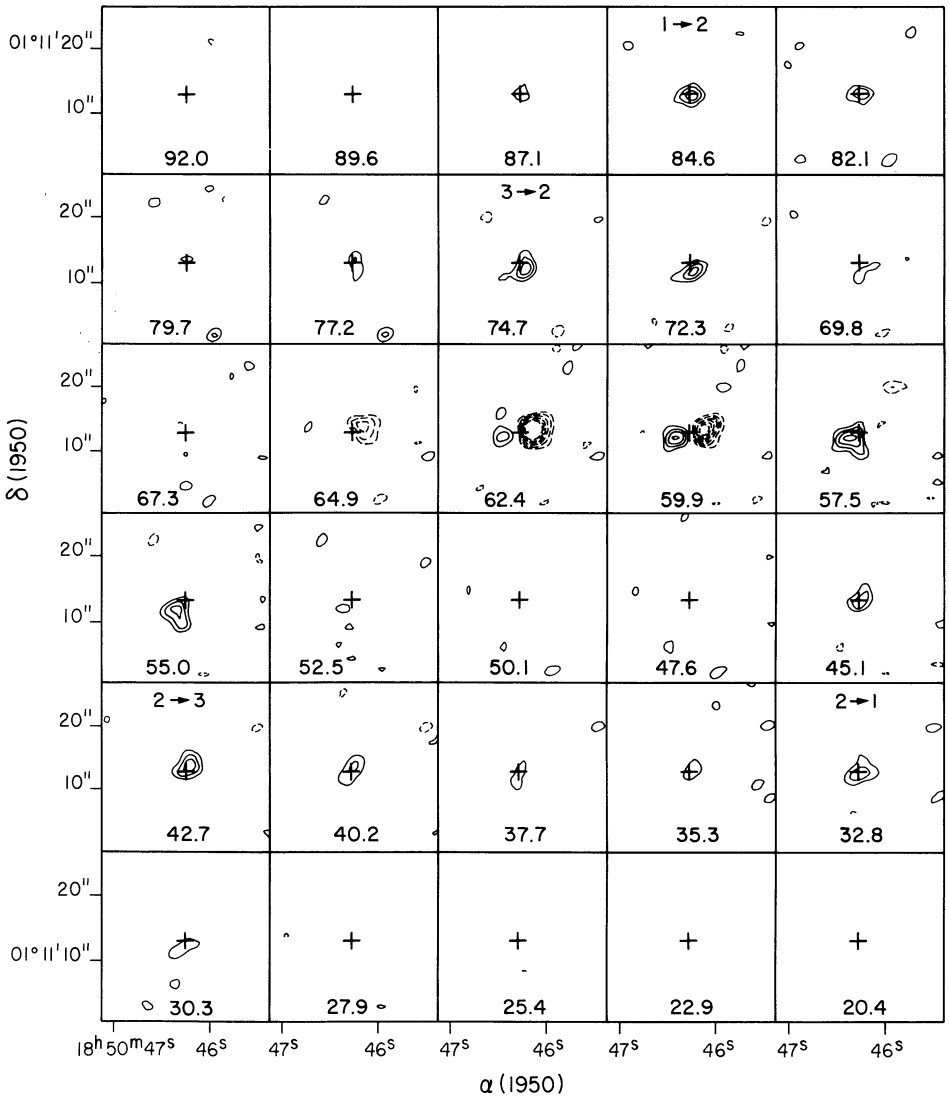

FIG. 3.—Channel maps of the (2, 2) line of ammonia. The LSR velocity is indicated at the bottom. Contour levels are −160, −140, −120, −100, −80, −60, −40, 40, 60, 80, 100, and 120 mJy beam^{-1}. Negative contours are dashed. The rms noise in the maps is 15 mJy beam^{-1}. The locations of the satellite hyperfine components, assuming a LSR velocity of 59.0 km s^{-1} for the main component, are indicated at the top by their $F' \rightarrow F$ values. Crosses mark the peak of the emission in the satellite lines.

region, which shows NH_3 in absorption. Second, the emission in the outer channel maps, which sample the emission from the HF satellite lines, arises from a region of small size that lies roughly in between the absorbing and emitting regions outlined by the main HF line. The position of the peak in the flux density of the satellite lines is shown with a cross in the maps of Figure 3.

Figure 4 shows the individual line maps of the (3, 3) inversion transition of NH_3 in the velocity range from 91.8 km s^{-1} to 18.2 km s^{-1}; the channel width is 2.45 km s^{-1}. The main HF line is detected in emission across the whole source. The satellite HF lines are also detected in emission but arising from a small central region; the peak in its flux density coincides with that of the (2, 2) HF satellite lines. This position is marked with a cross in the maps of Figure 4.

IV. ANALYSIS

The spectra of the NH_3 emission toward G34.3+0.2 have an exceptional shape: the (2, 2) inversion transition exhibits the main line either in absorption or emission and the satellite lines only in emission, while the (3, 3) inversion transition exhibits only emission features. This spectral appearance can be most simply explained if there is a blend, within a synthesized beam, of an emitting region of hot molecular gas and an absorbing region of cold gas in front of a continuum source. The lack of absorption in the (3, 3) inversion lines suggests that the absorbing gas has small opacities in the high-excitation ($J \geq 3$) inversion transitions of ammonia. The emission lines, principally those in the satellite HF lines, reflect the conditions of the hot gas, while the absorption line reflects the conditions of the cold gas.

In a simple model of two uniform components of molecular gas having constant excitation conditions, the observed brightness temperature at each position in the line maps and at the radial velocity v, $T_L(v)$, is given by the equation

$$T_L(v) = (T_H f_H - T_0 X_{0H}) \times \{1 - \exp[-\tau_H(v)]\} + (T_C f_C - T_0 X_{0C}) \times \{1 - \exp[-\tau_C(v)]\}, \quad (1)$$

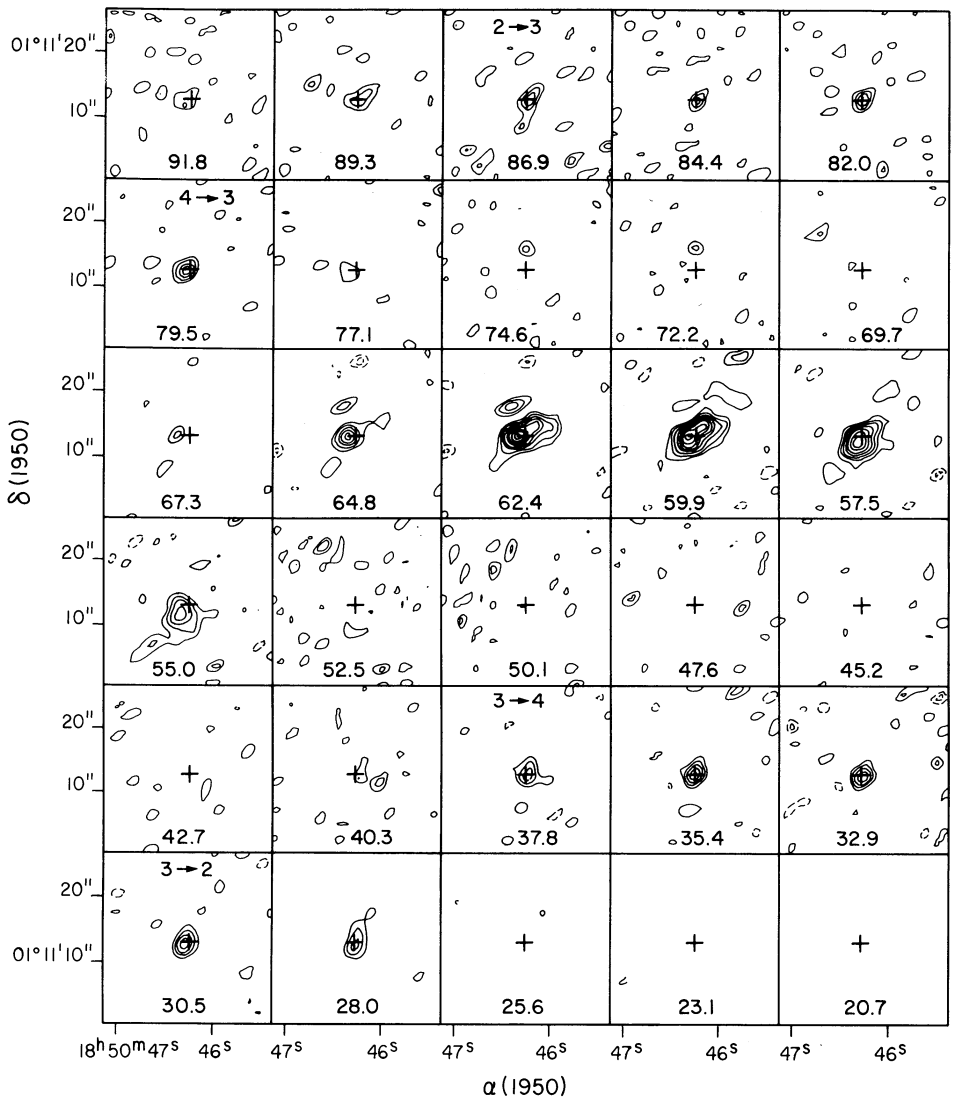

FIG. 4.—Same as Fig. 2, for the (3, 3) line of ammonia. Contour levels are −60, −40, 40, 60, 80, 100, 120, 140, 160, 180, and 200 mJy beam^{-1}. The rms noise in the maps is 17 mJy beam^{-1}.

where T_H and T_C, f_H and f_C, and $\tau_H(v)$ and $\tau_C(v)$ are the excitation temperatures, the beam-filling factors, and the optical depths of the hot and cold molecular gas, respectively; T_0 is the beam-averaged continuum brightness temperature; and X_{0H} and X_{0C} are the fraction of the continuum covered by the hot and cold gas, respectively. In particular for G34.3+0.2, the hot (emitting) cloud lies beside or behind the adjacent H II region (Andersson and Garay 1986); thus, throughout the remainder of this paper, we will assume that $X_{0H} = 0$. Figure 5 shows model spectra of the (2, 2) and (3, 3) lines of ammonia computed from the simple model, assuming $T_H = 185$ K, $T_C = 18$ K, $T_0 = 770$ K, $f_H = 0.25$, $f_C = 1.0$, $X_{0H} = 0$, and $X_{0C} = 0.35$. The total optical depth of the (3, 3) inversion transition was taken to be 39 and 0.06 for the hot and cold gas, respectively (see §§ IV*a*[i] and IV*b*[i]). These spectra closely reproduce those observed toward the western region of G34.3+0.2, showing that this simple model can accurately explain the observations.

In the following analysis, in which we aim to determine physical parameters of the molecular gas from their observed spectrum, we will divide the ammonia source toward G34.3+0.2 into three lines of sight (see Fig. 8): A, to the west, which shows the (2, 2) main HF line in absorption but the (3, 3) main HF line in emission; B, whose center is shown with a cross in Figures 3 and 4, which exhibits strong emission in the satellite HF lines of the (2, 2) and (3, 3) inversion transitions but weak or absent emission in the (2, 2) main HF line; and C, to the east, which exhibits both the (2, 2) and (3, 3) inversion lines in emission. From the observations of the main and satellite HF lines of an inversion transition of NH_3, we first determine its optical depth. Then, from the optical depths of two inversion transitions, we determine a rotational temperature between the molecular levels involved.

a) Line of Sight A (Bright H II *Region)*

The line of sight A passes through the head of the bright, cometary-shaped, compact H II region. Toward this region, the main HF line of the (2, 2) inversion transition, as well as the main HF line of the (1, 1) transition (KHR; Churchwell 1988),

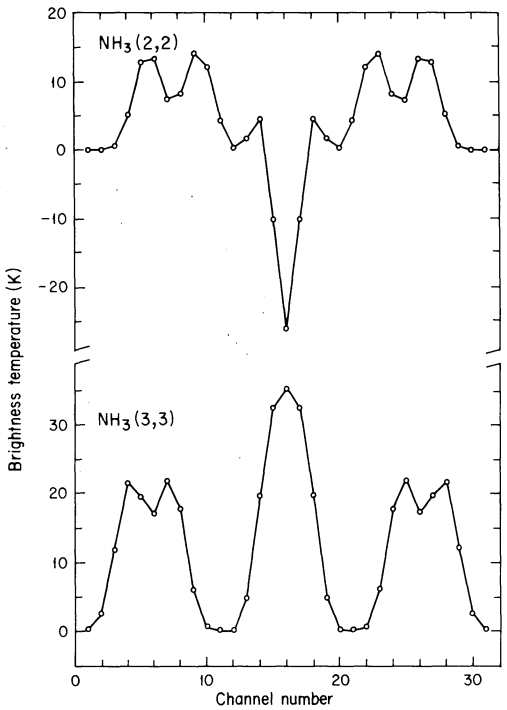

FIG. 5.—Model profiles of the (2, 2) and (3, 3) lines of ammonia. The model assumes the presence, within a beam, of a hot component of molecular gas, a bright radio continuum source and an extended and cold component of molecular gas. (See text for the adopted values of the temperatures and beam-filling factors.)

are detected in absorption. The (3, 3) main HF line is, however, present in emission.

i) *Absorbing Gas*

Our observations of the (2, 2) main HF component and those of the (1, 1) main HF component can be combined to derive physical parameters of the absorbing gas. Assuming that the most important contribution to the observed line brightness temperature in these transitions arises from the absorption of the bright continuum source by the cold gas, equation (1) gives

$$T_L(N, N; m) = -T_0 X_{0C}\{1 - \exp[-\tau_C(N, N; m)]\}, \quad (2)$$

where N indicates the inversion transition ($N = 1$ or 2), and m denotes its main HF component. Using the values observed for the (2, 2) main HF component [$T_L(2, 2; m) = -62 \pm 4$ K and $T_0 = 751 \pm 4$ in a 3.″0 beam (this paper)], the values observed for the (1, 1) main HF component [$T_L(1, 1; m) = -90$ K in a 3.″8 beam (Churchwell 1988) and $T_0 = 541$ in a 3.″7 beam (KHR)], and equation (2), we obtain

$$\{1 - \exp[-\tau_C(1, 1; m)]\}/\{1 - \exp[-\tau_C(2, 2; m)]\} = 2.1 .$$

From this expression, using the value of $\tau_C(1, 1; m)$ derived by KHR from the ratio of strengths of the HF lines of the (1, 1) transition, of 1.05, we obtain $\tau_C(2, 2; m) = 0.37 \pm 0.04$. The filling factor for the cold gas in front of the bright H II region, X_{0C}, is then ~ 0.3.

The rotational temperature between the (1, 1) and (2, 2) levels can be expressed in terms of the (1, 1; m) and (2, 2; m) optical depths by the equation (see Reid, Myers, and Bieging 1986)

$$T_R(2, 2; 1, 1) = -41.5\left\{\ln\left[\frac{9T_{ex}(2, 2)\nu(1, 1)0.500\tau(2, 2; m)}{20T_{ex}(1, 1)\nu(2, 2)0.796\tau(1, 1; m)}\right]\right\}^{-1} \text{K}, \quad (3)$$

where $T_{ex}(N, N)$ and $\nu(N, N)$ are the excitation temperature and frequency of the (N, N) transition. Assuming equal excitation temperatures and using the previously determined value of the opacities, we derive a rotational temperature for the absorbing gas, T_R^C, of 18 ± 3 K.

The opacity of the cold gas in the (3, 3; m) HF line can be estimated using the previously derived values of the opacity in the (2, 2; m) HF line and of the rotational temperature. Assuming $T_R^C(3, 3; 2, 2) = T_R^C(2, 2; 1, 1)$, we find that $\tau_C(3, 3; m) \sim 0.05$. We conclude that the absorbing gas has moderate and negligible opacities at the frequencies of the main HF line of the (2, 2) and (3, 3) inversion transitions, respectively.

The average velocity of the absorbing gas, determined by fitting a Gaussian profile to the spectrum of the (2, 2; m) line obtained by integration of the flux density in the line maps over the angular extent of absorption feature, is 61.7 ± 0.3 km s^{-1}. This value is in good agreement with the velocity of the absorption feature determined from the observations of the (1, 1) line, of ~ 61.2 km s^{-1} (KHR).

ii) *Emitting Gas*

Since the opacities of the cold gas in the lines of the (3, 3) inversion transition are much less than 1, the absorption of the continuum source by the cold gas, at those frequencies, is not the dominant term in expression (1). In this case, the line brightness temperature can be written as

$$T_L(3, 3; k) = T_H f_H \times \{1 - \exp[-\tau_H(3, 3; k)]\} + (T_C f_C - T_0 X_{0C}) \times \tau_C(3, 3; k), \quad (4)$$

where $k = m$ or s. At the position of the strongest absorption in the (2, 2; m) line, we measured a flux density in the (3, 3; m) line of 110 ± 17 mJy beam^{-1}, implying $T_L(3, 3; m) \sim 25 \pm 4$ K. The positive value indicates that the contribution to the line brightness temperature from the hot gas, lying beside or behind the H II region, is larger than the absorption by the cold gas. Replacing the values of $X_{0C} = 0.27$, $T_0 = 751$ K, and $\tau_C(3, 3; m) = 0.048$, previously derived, and the observed value of $T_L(3, 3; m)$ in equation (4), we derive a lower limit to the excitation temperature of the hot gas of ~ 40 K. The actual value cannot be determined since the filling factor and opacity of the gas toward A are unknown.

In the line of sight A the (2, 2) satellite lines are either weakly detected in emission or undetectable. The lack of absorption in these lines gives further support to our suggestion that the absorption observed in the main line of the (2, 2) transition arises in a cold gas of low optical depth. The optical depth of the cold gas in the (2, 2) satellite components, $\tau_C(2, 2; s)$, expected from the opacity in the main component assuming LTE conditions, is ~ 0.02. Thus, absorption by the cold gas at the frequencies of the (2, 2) satellite lines should be negligible, in agreement with the observations that do not show absorption in the satellite lines.

b) Line of Sight B (Ultracompact NH_3 *Core)*

The line of sight B exhibits the strongest emission in the HF satellite lines of the (2, 2) and (3, 3) inversion transitions over

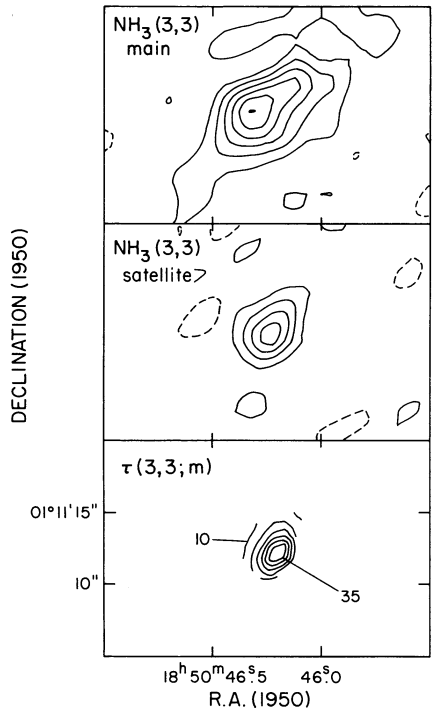

FIG. 6.—Contour maps of the emission and optical depth of the NH_3 (3, 3) inversion transition toward G34.3+0.2. The resolution, indicated by the shaded ellipse, is 3".2 × 3".0, P.A. = −53°. *Top*: Main line emission. Contour levels are −30, 30, 60, 90, 120, 150, and 180 mJy beam^{-1}. *Middle*: Satellite line emission. Contour levels are −20, 20, 40, 60, and 80 mJy beam^{-1}. *Bottom*: Main line optical depth. Contour levels are 10, 15, 20, 25, 30, and 35.

the whole source, implying that this is the region of the compact molecular core with the largest optical depth. Figure 6 shows a map of the integrated emission in the satellite lines of the (3, 3) inversion transition. Most of the HF satellite emission arises from an *ultracompact core* with a deconvolved size of 1".6. The position of the peak emission in the satellite lines is displaced about 2" to the east from the peak position of the continuum emission. The average radial velocity of the gas in the ultracompact core, determined by simultaneously fitting four Gaussian profiles, with fixed velocity separations, to the integrated flux density in the satellite HF lines, is 58.9 km s^{-1}.

i) *Opacities*

All the HF components of the (3, 3) inversion transition are detected in emission, which allows a direct estimate of their optical depths. Figure 6 (*bottom panel*) shows a map of the opacity of the (3, 3) main line, computed from the ratio of the line maps of the main and satellite components, assuming equal beam-filling factors and equal values of the excitation temperature. We have neglected absorption in the (3, 3) line by the cold gas. At the position of maximum flux density in the satellite lines, we find $\tau_H(3, 3; m) \sim 37$; hence, $\tau_H(3, 3; s) \sim 1.1$. We notice, however, that these values may correspond to upper limits if $T_L(3, 3; m)$ is affected from absorption by cold foreground gas. In the following analysis we will assume, to be conservative, that in the line of sight B the value of $\tau_H(3, 3; m)$ is within the range between 30 and 35; hence, $\tau_H(3, 3; s)$ is in the range from 0.91 to 1.06.

Our observations show that the (2, 2) main HF line in the line of sight B is absent or weakly absorbed, which is probably due to a near cancellation of the contributions to the line brightness temperature from the hot emitting gas and from the absorption of the continuum emission by the cold gas. On the other hand, the (2, 2) satellite HF lines show strong emission that suggests that the cold absorbing gas has small opacities at the frequencies of these lines. The absence of the (2, 2; *m*) line prevents us from computing the optical depth of the (2, 2) inversion components directly from their line intensity ratios. The optical depth of the (2, 2) satellite lines can be determined, using the observed ratio of line brightness temperature of the (3, 3) and (2, 2) HF satellite lines and the value of the optical depth of the (3, 3; *s*) lines previously derived, from the equation

$$\tau_H(2, 2; s) = -\ln\left[1 - \frac{T_L(2, 2; s)}{T_L(3, 3; s)} \times \{1 - \exp[-\tau_H(3, 3; s)]\}\right], \quad (5)$$

which assumes equal beam-filling factors and equal excitation temperatures for the (2, 2) and (3, 3) lines and that the absorption by the cold gas is negligible, an approximation quite accurate for the satellite lines. At the position of maximum flux density in the satellite lines $T_L(2, 2; s) = 21.5 \pm 1.6$ K and $T_L(3, 3; s) = 24.0 \pm 1.5$ K, values which correspond to the average of the observed peak brightness temperatures in each of the four HF satellite components. The 1 σ errors are thus smaller (typically by a factor of 2) than the rms noise in a single line channel. For $\tau_H(3, 3; s)$ in the range of 0.91 to 1.06, we then find that $\tau_H(2, 2; s)$ is in the range of 0.77–0.98.

ii) *Rotational Temperature*

Using the optical depth of the satellite transitions, the rotational temperature can be derived from the expression

$$T_R(3, 3; 2, 2) = -59.6\left\{\ln\left[\frac{20T_{ex}(3, 3)0.052\nu(2, 2)\tau(3, 3; s)}{63T_{ex}(2, 2)0.027\nu(3, 3)\tau(2, 2; s)}\right]\right\}^{-1} \text{K}. \quad (6)$$

Assuming equal excitation temperatures for the (2, 2) and (3, 3) levels and using the values of the optical depths of the satellite lines derived above, we determine that the rotational temperature of the ultracompact molecular structure associated with G34.3+0.2 is 185^{+75}_{-45} K.

c) Line of Sight C

The line of sight C passes through one of the weak ultracompact H II regions associated with the compact molecular core. The ammonia spectrum from this region shows moderate emission in the main lines of the (2, 2) and (3, 3) inversion transitions and weak emission in the HF satellites. The lack of absorption suggests that the H II region is either in front of the molecular gas or that its beam-averaged continuum brightness temperature is very small. Neglecting the absorption by the weak continuum source and the emission by the cold gas, equation (1) can be written as

$$T_L(N, N; k) = T_H f_H\{1 - \exp[-\tau_H(N, N; k)]\}, \quad (7)$$

where $k = m$ or s.

i) *Opacities*

The optical depths of the (2, 2) and (3, 3) inversion transitions can be derived directly from the intensity ratio of their HF components using equation (7). From the observed flux densities per beam in the main and satellite lines of the (2, 2)

inversion transition, of 106 ± 13 and 30 ± 8 mJy beam^{-1}, respectively, we derive $\tau_H(2, 2; m) \sim 5.1 \pm 1.2$. Similarly from the observed flux densities per beam in the main and satellite lines of the (3, 3) transition of 120 ± 17 and 25 ± 9 mJy beam^{-1}, respectively, we obtain $\tau_H(3, 3; m) \sim 7.7 \pm 2.3$. The opacities in the satellite lines, derived from the opacities in the main lines, assuming LTE conditions, are $\tau_H(2, 2; s) \sim 0.33 \pm 0.08$ and $\tau_H(3, 3; s) \sim 0.23 \pm 0.07$. An independent estimate of the opacity of the (2, 2; s) lines can be obtained using equation (5). Replacing in this equation the observed value of the ratio $T_L(2, 2; s)/T_L(3, 3; s)$, of ~ 1.20, and the value of the opacity in the (3, 3; s) line derived above, we find $\tau(2, 2; s) = 0.28 \pm 0.08$, in good agreement with the value derived directly from the line intensity ratio.

ii) *Rotational Temperature*

Assuming equal excitation temperature for the (2, 2) and (3, 3) transition and using the opacities derived above, equation (6) gives a rotational temperature for the emitting gas in the line of sight C of $\sim 70 \pm 25$ K.

V. DISCUSSION

In this section, we discuss the characteristics and physical conditions of the emitting and absorbing gas as a whole and propose a simple scenario to explain the cloud dynamics. Observed and derived parameters of the ammonia gas in the different regions of G34.3+0.2 defined in § IV are summarized in Table 1.

a) Emitting Gas

i) *Morphology*

The appearance of the warm ammonia cloud toward G34.3+0.2 is best delineated by the emission in the main line of the (3, 3) transition, which is not affected by absorption from the cold foreground gas. The shape of the source is roughly that of an ellipse with a deconvolved major axis of $\sim 7''.3$, oriented in a direction $\sim 55°$ west from north, and a deconvolved minor axis of $\sim 3''$. This source, also referred to as the compact core (see Henkel, Wilson, and Mauersberger 1987), is at the center of the extended, less dense molecular core mapped by Heaton *et al.* (1985). The position of the peak in the line emission from the (3, 3) main HF component, $\alpha = 18^h50^m46^s.23$, $\delta = 1°11'12''.9$, is displaced approximately $2''$ to the east of the peak in the continuum emission, as already found by Andersson and Garay (1986). The peak flux density, in a $3''.2 \times 3''.0$ beam, is 0.19 ± 0.01 Jy beam^{-1}, and the total flux density is 0.64 ± 0.04 Jy.

The warm molecular cloud itself exhibits a core-halo structure. The emission from the HF satellite lines of the (3, 3) inversion transition, which presumably samples a hotter and denser molecular component, arises from a region, of $\sim 1''.6$ in size, near the center of the warm cloud. The position of maximum emission in the HF satellite lines is at $\alpha = 18^h50^m46^s.23$, $\delta = 1°11'12''.6$. The emission from the highly excited lines of ammonia observed by Henkel, Wilson, and Mauersberger (1987) most likely arises from this ultracompact molecular core.

ii) *Kinetic Temperature*

In general, the rotational temperature of the NH_3 emission sets a lower limit to the kinetic temperature of the gas. The rotational temperature at the center of the compact molecular core, derived from the line flux densities of the (2, 2) and (3, 3) satellite lines, is 185^{+75}_{-45} K. Henkel, Wilson, and Mauersberger (1987), from a multilevel study of highly excited lines of ammonia, determined an average value for the rotational temperature of 225 K, in good agreement with our determination for the temperature of the ultracompact core. We suggest that the hot emission arises in a layer of gas heated and compressed by the associated bright compact H II region.

Several observations show that the average temperature of the warm ammonia cloud is about two to three times smaller than that in its ultracompact core. From CH_3CN observations, Andersson (1985) determined a kinetic temperature of 90 K, while Andersson and Garay (1986) determined an excitation temperature of ~ 60 K from NH_3 observations. We derive a rotational temperature of $\sim 70 \pm 25$ K at the southeast edge of the cloud, in agreement with previous determinations.

iii) *Column Densities and Densities*

Assuming an LTE population for all ammonia levels, we can estimate the total column density of NH_3 from the optical depth of an inversion transition, $\tau(J, K)$, and the rotational temperature, T_R, using the expression

$$N(\mathrm{NH_3}) = \frac{1.65 \times 10^{14}}{\nu_{\mathrm{GHz}}} \frac{J(J+1)}{g_K K^2 (2J+1)} \times \Delta V \tau(J, K) Q T_{\mathrm{ex}} \exp\left(\frac{E}{kT_R}\right), \quad (8)$$

where Q is the partition function, g_K is the statistical weight of the ortho ladders, E is the energy of the (J, K) level above the ground state, ΔV is the line width in km s^{-1}. If the metastable and nonmetastable levels of NH_3 are populated and $T_R \gg 20$ K, as is probably the case for the warm and hot molecular gas toward G34.3+0.2, $Q = 41(T_R/100\ \mathrm{K})^{3/2}$ (Genzel *et al.* 1982). The column densities of ammonia toward the core and the halo of the warm molecular cloud, obtained from equation (8) using the values of the total optical depth in the (3, 3) transition, the rotational temperatures derived in § IV, and $T_{\mathrm{ex}} = T_R$, are $\sim 6 \times 10^{18}$ and 2×10^{17} cm^{-2}, respectively.

The ammonia densities (col. [6] of Table 1) are derived from the column densities assuming that the emitting gas has a spherical geometry, with angular sizes of $1''.6$ for the ultracompact core and of $2''.8$ for the SE region of the warm molecular structure. Assuming a $n(NH_3)/n(H_2)$ fractional abundance for the hot gas of 10^{-6} (Henkel, Wilson, and Mauersberger 1987) yields a molecular hydrogen density for the ultracompact core

TABLE 1

PARAMETERS OF AMMONIA GAS TOWARD G34.3+0.2

Line of Sight (1)	Δv (km s^{-1}) (2)	$\tau(3, 3)$ (3)	T_R (K) (4)	$N(NH_3)$ (cm^{-2}) (5)	$n(NH_3)$ (cm^{-3}) (6)
A (absorption)	2.4 ± 0.7	0.05 ± 0.01	18 ± 3	2×10^{15}	$\sim 10^{-3}$
B	7.5 ± 1.2	34–39	185^{+75}_{-45}	$(6-7) \times 10^{18}$	~ 70
C	3.4 ± 1.4	8.6 ± 2.6	70 ± 25	2×10^{17}	~ 1

of $\sim 7 \times 10^7$ cm^{-3}. Support for the presence of such large density toward G34.3+0.2 is given by the detection of several nonmetastable lines of ammonia (Henkel, Wilson, and Mauersberger 1987), which require densities on the order 10^8–10^9 cm^{-3} to be collisionally populated.

iv) *Overall Cloud Structure*

There is considerable evidence for the presence of density and temperature gradients, from scales ranging from a few parsecs to a few hundredths of parsecs, within the molecular gas associated with G34.3+0.2. Table 2 lists physical parameters of a hierarchical arrangement of ammonia structures. The temperatures and densities as a function of distance can be reasonably described with power-law expressions of the form $(T/\mathrm{K}) \simeq 21(d/\mathrm{pc})^{-0.6\pm0.1}$ and $[n(\mathrm{H_2})/\mathrm{cm^{-3}}) \simeq 5.5 \times 10^4 (d/\mathrm{pc})^{-1.7\pm0.4}$. These fits are shown in Figure 7.

The density gradients observed in the molecular gas of G34.3+0.2 are most likely due to the gravitational collapse of an extended, inhomogeneous, low density molecular cloud. We suggest the following scenario to explain the observations of the central region of this cloud. The warm compact molecular clump corresponds to a molecular disk structure that was formed from the collapse of a massive, rotating fragment embedded within the extended molecular cloud. Evidence for rotational motions of the emitting gas has been presented by KHR who measured, in the (1, 1) main HF line, a velocity gradient of 15 ± 6 km s^{-1} pc^{-1} over a 0.3 pc region, and by Heaton *et al.* (1989) who observed a similar shift in the position of the peak (3, 3) main HF line brightness temperature with velocity. This velocity shift is also present in our (3, 3) main HF line observations with the emission at $v_{\mathrm{LSR}} = 55.0$ km s^{-1} peaking to the south of the emission at 64.8 km s^{-1} (see Fig. 4). The elongated molecular structure detected in the $J = 1$–0 transition of HCO^+ by Carral, Welch, and Wright (1987) is more extended and shows different orientation than the warm ammonia core, but also has its southern parts blueshifted with respect to its northern ones. In contrast, the ionized gas (Garay, Rodríguez, and van Gorkom 1986) shows a velocity gradient with opposite sense than that of the molecular one, that is, the southern parts are redshifted with respect to the northern ones. The origin of this peculiar kinematic behavior is unknown.

Most of the molecular mass at the center of this disk, which perhaps had the lowest angular momentum, further collapsed to form massive stars that are presently exciting the cometary ultracompact H II region. The hot and dense ultracompact core observed at the center of the disk corresponds to a dense layer of molecular gas that is near and around the recently formed star and that is heated and further compressed by the adjacent ultracompact H II region. Figure 8 shows a schematic representation of the morphology of the molecular and ionized gas toward G34.3+0.2, as proposed by us.

TABLE 2

PHYSICAL PARAMETERS OF DIFFERENT AMMONIA STRUCTURES TOWARD G34.3+0.2

Component	L (pc)	T_{ex} (K)	$n(\mathrm{H_2})$ (cm^{-3})	Reference
Extended envelope	3.7	9	5×10^3	1
Molecular core	1.7	18	4×10^4	1
Warm compact core	0.1	60	6×10^5	2
Hot ultracompact core	0.03	185	7×10^7	3

REFERENCES.—(1) Heaton *et al.* 1985; (2) Andersson and Garay 1986; (3) this paper.

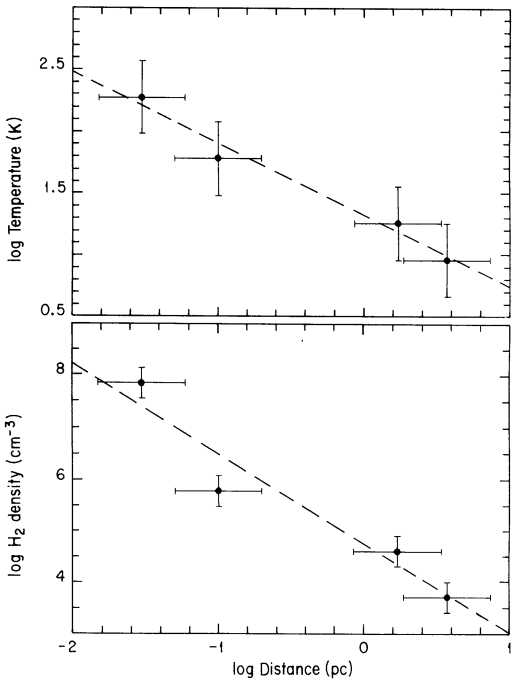

FIG. 7.—Temperature (*top*) and density (*bottom*) as a function of distance from the exciting stars for the G34.3+0.2 region. The data are taken from Table 2. The dashed lines are least-squares linear fits to the data points (see text).

b) Absorbing Gas

The absorption feature seen in the main line of the (2, 2) transition, but absent in the main line of the (3, 3) transition, arises in a cold gas of moderate opacity in front of the brightest continuum source toward G34.3+0.2. The optical depths of

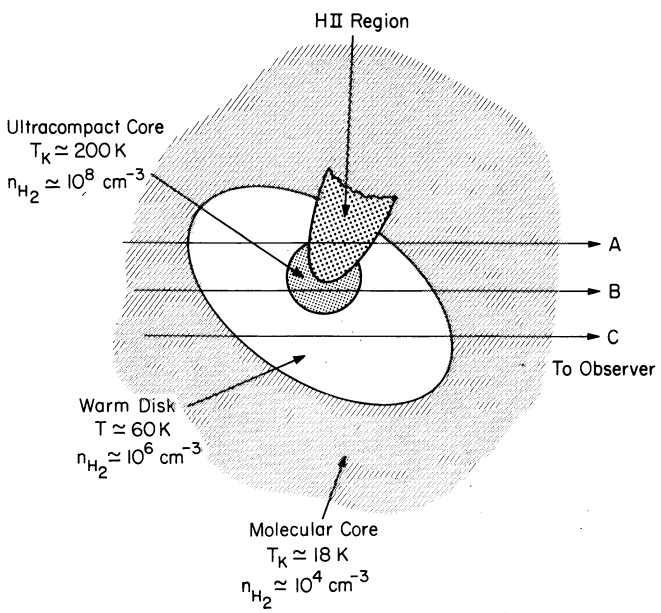

FIG. 8.—Schematic representation of the morphology of the molecular and ionized gas toward G34.3+0.2.

the absorbing gas in the main HF lines of the (1, 1) and (2, 2) transitions, derived from our data and that reported by KHR, are ~ 1.0 and 0.37, respectively. The rotational temperature, between those two states, is 18 K. The expected optical depth in the (3, 3) main HF line is negligible ($\tau_C \sim 0.05$); thus, the cold gas does not affect the emission from the warm and dense gas from the molecular core. The column density of the ammonia gas in the absorbing cloud, determined from equation (8) using $Q = 8(T_R/100\ \mathrm{K})$ (Genzel *et al.* 1982) and $T_{ex} = T_R$, is 2.1×10^{15} cm^{-2}. Since the path length of the absorbing gas is not known, the density of ammonia cannot be derived in a straightforward manner from the column density. Assuming that the length of the absorbing cloud is about one-half the diameter of the 18 K cloud as measured by Heaton *et al.* (1985) gives $n(NH_3) \sim 8 \times 10^{-4}$ cm^{-3}. Further, assuming that in the cold gas $[NH_3]/[H_2] \sim 10^{-7}$, as obtained for interstellar dark clouds (Ungerechts, Walmsley, and Winnewisser 1980; Benson and Myers 1983), we derive a molecular density for the absorbing gas of $\sim 10^4$ cm^{-3}.

The absorbing gas, at a velocity of 61.7 km s^{-1}, is redshifted with respect to the velocity of the warm molecular cloud by ~ 3 km s^{-1}. KHR, from a study of the (1, 1) line, suggested that the absorbing material might be part of the remnant gas that is still gravitationally collapsing onto the recently formed central star (or stars). The low temperature and low densities of the absorbing gas, derived in this paper, do not support models in which the absorption feature arises in gas immediately around and accreting onto the H II region since such gas is expected to be hotter and denser than the gas in the warm molecular cloud. We attribute the absorption feature to a foreground cloud, of $n(H_2) \sim 10^4$ cm^{-3} and $T_K \sim 18$ K, which is moving toward the core of the cloud (see also Matthews *et al.* 1987). The absorbing gas is most likely part of the extended molecular core mapped by Heaton *et al.* (1985).

VI. CONCLUSIONS

We mapped, with the VLA, the ammonia emission, in the lines of the $(J, K) = (2, 2)$ and $(J, K) = (3, 3)$ inversion transitions, toward the warm molecular cloud associated with the compact H II region G34.3+0.2. The main results and conclusions presented in this paper are summarized below.

1. The main HF line of the (2, 2) inversion transition is detected in absorption in the western half of the source and in emission in the eastern half. The main HF line of the (3, 3) inversion transition is detected in emission over the whole source. The HF satellite lines of the (2, 2) and (3, 3) inversion transitions are detected only in emission. The appearance of the spectra in the western region of the source, exhibiting emission and absorption features, is interpreted as due to a blend, within a synthesized beam, of two components of molecular material: a warm, optically thick, cloud of gas and cold component of gas of moderate optical depths in front of a continuum radio source.

2. The warm molecular cloud exhibits a core-halo structure. The emission in the main HF component of the (3, 3) transition, which samples the whole warm cloud, arises from a disklike structure of $\sim 7''.3 \times 2''.8$ in size, elongated in a direction oriented $\sim 55°$ west of north. The emission from the HF satellite lines of the (2, 2) and (3, 3) inversion transitions, which presumably sample denser and hotter molecular gas, arise from an ultracompact region, of $\sim 1''.6$ in size, near the center of the warm molecular cloud. The ultracompact core is displaced $\sim 2''$ to the east of the bright cometary H II region within the complex.

3. The rotational temperature increases from about 70 K near the edges of the warm molecular core to ~ 185 K at the position of the ultracompact molecular core. The column density of ammonia increases from $\sim 2 \times 10^{17}$ cm^{-2}, at the SE position, to $\sim 6 \times 10^{18}$ cm^{-2} at the position of the hot ultracompact core; the ammonia densities are ~ 1 cm^{-3} and 70 cm^{-3}, respectively.

4. The hydrogen molecular density in the ultracompact core, assuming $n(NH_3)/n(H_2) = 10^{-6}$, is $\sim 7 \times 10^7$ cm^{-3}. This H_2 density, one of the largest so far derived in regions associated with star formation, is of the order of the critical densities required to populate the nonmetastable levels of ammonia (of $\sim 10^8$–10^9 cm^{-3}). The emission from the nonmetastable, and the highly excited metastable, inversion transitions observed by Henkel, Wilson, and Mauersberger (1987) most likely arises from the ultracompact core.

5. The absorption line, at 61.7 km s^{-1}, arises from a gas of low optical depth in front of the brightest H II region within the complex. The rotational temperature of this gas is 18 K. We suggest that this gas is part of the extended, low-density molecular core, mapped by Heaton *et al.* (1985), that surrounds the H II regions.

6. The following scenario is suggested to explain the characteristics of the gas at the center of the G34.3+0.2 cloud. The warm disklike molecular clump may be the result of the gravitational collapse of a rotating and massive fragment that was embedded in a low density molecular cloud. A central massive star was formed at the center of this disk, producing a compact H II region. The molecular material around the ionized gas is heated and further compressed, producing a hot ultracompact molecular core.

G. G. is the grateful recipient of an Henri Chrétien Award. L. F. R. acknowledges support from a Guggenheim Fellowship. This research has been partially supported by the Chilean FONDECYT under grant 0502/88.

REFERENCES

Andersson, M. 1985, in *Proc. ESO-IRAM-Onsala Workshop on (Sub)Millimeter Astronomy*, ed. P. A. Shaver and K. Kjär (*ESO Proceedings 22*), p. 353.
Andersson, M., and Garay, G. 1986, *Astr. Ap.*, **167**, L1.
Benson, P. J., and Myers, P. C. 1983, *Ap. J.*, **270**, 589.
Carral, P., Welch, W. J., and Wright, M. C. H. 1987, *Rev. Mexicana Astr. Af.*, **14**, 506.
Churchwell, E. 1988, in *Galactic and Extragalactic Star Formation*, ed. R. E. Pudritz and M. Fich (Dordrecht: Kluwer), p. 275.
Garay, G., Reid, M. J., and Moran, J. M. 1985, *Ap. J.*, **289**, 681.
Garay, G., Rodríguez, L. F., and van Gorkom, J. H. 1986, *Ap. J.*, **309**, 553.
Gaume, R. A., and Mutel, R. L. 1987, *Ap. J. Suppl.*, **65**, 193.
Genzel, R., and Downes, D. 1977, *Astr. Ap. Suppl.*, **30**, 145.
Genzel, R., Downes, D., Ho, P. T. P., and Bieging, J. 1982, *Ap. J. (Letters)*, **259**, L103.
Heaton, B. D., Matthews, N., Little, L. T., and Dent, W. R. F. 1985, *M.N.R.A.S.*, **217**, 485.
Heaton, B. D., Little, L. T., and Bishop, I. S. 1989, *Astr. Ap.*, **213**, 148.

Henkel, C., Wilson, T. L., and Mauersberger, R. 1987, *Astr. Ap.*, **182**, 137.
Keto, E., Ho, P. T. P., and Reid, M. J. 1987, *Ap. J. (Letters)*, **323**, L117 (KHR).
Matthews, N., Little, L. T., MacDonald, G. H., Andersson, M., Davies, S. R., Riley, P. W., Dent, W.R. F., and Vizord, D. 1987, *Astr. Ap.*, **184**, 284.
Reid, M. J., and Ho, P. T. P. 1985, *Ap. J. (Letters)*, **288**, L17.
Reid, M. J., Myers, P. C., and Bieging, J. H. 1986, *Ap. J.*, **312**, 830.
Schwab, F. 1980, *Proc. Soc. Photo-Opt. Instr. Eng.*, **231**, 18.
Turner, B. E., Balick, B., Cudaback, D. D., Heiles, C., and Boyle, R. J. 1974, *Ap. J.*, **194**, 279.
Ungerechts, H., Walmsley, C. M., and Winnewisser, G. 1980, *Astr. Ap.*, **88**, 259.

GUIDO GARAY: Departamento de Astronomía, Universidad de Chile, Casilla 36-D, Santiago, Chile

LUIS F. RODRÍGUEZ: Instituto de Astronomía, UNAM, Apdo. Postal 70-264, 04510, México, D.F., México